Supporting information

Reversible Cu^{+}/Cu^{2+} Cycles Enable Enhanced Carrier Separation for Efficient Photocatalytic Ammonia Synthesis

Weiwei Shao, You Yang, Yang Shen, Chengbin Zhang, Yuanyuan Wang, Yingfei Hu, Yang Wu, Jun Hu, Junfa Zhu, Hangmin Guan, Xiaolong Zu, Xiaodong Li* and Xingchen Jiao**

Weiwei Shao, You Yang, Yang Shen, Yuanyuan Wang, Yingfei Hu, Hangmin Guan*
School of Materials Engineering, Jinling Institute of Technology, Nanjing 211169, China
E-mail: guan@jit.edu.cn

Yang Wu, Jun Hu, Junfa Zhu
National Synchrotron Radiation Laboratory, University of Science and Technology of China, Hefei 230026, China

Xiaolong Zu
Innovation Laboratory for Sciences and Technologies of Energy Materials of Fujian Province (IKKEM), Xiamen 361005, China

Xiaodong Li*
Max Planck Institute of Microstructure Physics, Weinberg 2, Halle 06120, Germany
Email: Xiaodong.li@tu-dresden.de

Chengbin Zhang, Xingchen Jiao*
Key Laboratory of Synthetic and Biological Colloids, Ministry of Education, School of Chemical and Material Engineering, Jiangnan University, Wuxi 214122, China
email: xcjiao@jiangnan.edu.cn

Experimental section

Synthesis of pristine $BiVO_4$ nanoplates:

In a typical procedure, bismuth nitrate pentahydrate (1.0 mmol) and sodium dodecyl sulfate (0.3 g) were added to acetic acid solution (0.8 M, 15 mL) and the mixture was stirred thoroughly to form solution A. For solution B, ammonium vanadate (1.0 mmol) was added to sodium hydroxide solution (1.0 M, 10 mL) with stirring maintained until a homogeneous mixture was achieved. Thereafter, solution B was added dropwise to solution A and the resultant mixture was stirred for a while. Subsequently, the pH was adjusted to 7, and the mixture was subsequently transferred into a Teflon-lined autoclave, sealed and heated at 160 °C for 12 h. The final product was collected by centrifuging, washed with ethanol and deionized water for many times, and then dried in the vacuum.

Synthesis of Cu-doped $BiVO_4$ nanoplates:

The synthesis of Cu-doped $BiVO_4$ nanoplates followed the same synthetic process as that of fabricating pristine $BiVO_4$ nanoplates, with the exception that cupric sulfate ($CuSO_4$) was added at varying molar ratios (2%, 5%, 10%) to the mixture after the pH was adjusted to 7. The mixture was stirred for a further 20 minutes, subsequently transferred into a Teflon-lined autoclave, sealed and heated at 160 °C for 12 h. The final product was collected by centrifuging, washed with ethanol and deionized water for many times, and then dried in the vacuum.

Characterization:

Transmission electron microscopy (TEM) images were acquired using a JEOL JEM-2100Plus. The high-resolution TEM images and elemental mapping images were obtained using a JEOL JEM-F200. X-ray diffraction (XRD) patterns were recorded on a Rigaku Miniflex 600 X-ray diffractometer with Cu Kα radiation (λ = 1.54178 Å). Scanning electron microscope (SEM) images were obtained using a HITACHI SU8010 field-emission scanning electron microscope. X-ray photoelectron spectroscopy (XPS) spectra were acquired on a Thermo NEXSA G2 system with Al Kα ($h\nu$ = 1486.6 eV) as the excitation source. The binding energies obtained in the XPS spectral analysis were calibrated for sample charging by referencing C 1s to 284.8 eV. UV−vis diffuse reflectance spectroscopy was measured on a SHIMADAZU UV 2600 UV−vis

spectrophotometer. Raman spectra were detected by HORIBA Scientific S3000 System, in which the excitation wavelength was at 532 nm. Photoluminescence (PL) spectra were obtained on an Edinburgh Instruments FLS-1000 time-resolved photoluminescence spectrometer. ^{1}H nuclear magnetic resonance (^{1}H NMR) measurements were conducted on a Bruker 600 MHz AVANCE NEO instrument. Synchrotron-radiation quasi *in-situ* XPS measurements were performed at the photoemission end-station at beamline BL11U in the National Synchrotron Radiation Laboratory (NSRL) in Hefei, China. *In-situ* Fourier-transform infrared (FTIR) measurements were conducted on Thermo Scientific Nicolet iS50, equipped with a commercial reaction chamber and an MCT detector cooled by liquid nitrogen. Photoelectrochemical measurements were conducted in a three-electrode system at an electrochemical station (CHI760E). The working electrode was prepared by spin-coating the slurry, which was formed by dispersing as-prepared samples into ethanol, onto the ITO glass. A platinum foil, Ag/AgCl electrode and Na_2SO_4 solution (0.2 M) were selected as the counter electrode, reference electrode, and the electrolyte, respectively. The Mott–Schottky measurements were carried out at different frequency (1.5, 2.0 and 2.5 kHz) and the electrochemical impedance spectra (EIS) were measured in the frequency range of 0.1 to 1000 kHz. For the charge separation efficiency in the bulk of semiconductor (η_{bulk}) measurements, Na_2SO_3 solution (0.2 M) were used as the electrolyte according to the previous report. [1]

Photocatalytic N_2 reduction measurements:

The photocatalytic N_2 reduction measurements were conducted in a sealed off-line reactor with external circulating water system to maintain a constant temperature. In the typical photocatalytic process, 50 mg of the photocatalyst was dispersed in a methanol-water solution with a volume ratio of 1%. The system was subsequently purged with high-purity nitrogen until saturated, and the photocatalytic nitrogen reduction test was conducted under irradiation from CEL-HXF300 Xe lamp (Beijing China Education Au-light Co., Ltd.). At predetermined time intervals, 2 mL aliquots of the reaction mixture were collected. The nitrogen fixation activity of the photocatalyst was evaluated using the Nessler's reagent method with an UV-6300 spectrophotometer (Shanghai MAPADA instruments Co., Ltd.). In detail, after removing the photocatalyst solids, 1 mL of the filtrate was transferred to a 25 mL colorimetric tube and

diluted with deionized water. Next, 0.5 mL of potassium sodium tartrate solution and 0.5 mL of Nessler's reagent was added in sequence, after which the mixture was vortexed thoroughly and allowed to stand for several minutes. The absorbance at 420 nm was measured and the product concentration was quantified based on a pre-established calibration curve. For ^{1}H-NMR measurement, sulfuric acid was used to regulate pH of solution and DMSO-d_6 was used for a spin-lock field. [2]

DFT calculation details:

Density functional theory (DFT) calculations were carried out on a Vienna Ab initio Simulation Package (VASP). [3] The exchange-correlation potential was described by the generalized gradient approximation (GGA) within the framework of Perdew-Burke-Ernzerhof (PBE) functional. [4] DFT-D3 method was employed to calculate the van der Waals (vdW) interaction. [5] The parameters of dipole correction were applied for the calculation of slab models. Electronic energies were computed with the tolerance of 1×10^{-5} eV and total force of 0.02 eV·Å^{-1}. A kinetic cutoff energy of 450 eV was adopted. The $BiVO_4$ slabs were modeled using the corresponding exposed surface along $[0\bar{3}1]$ direction with a vacuum space of 15 Å in z directions to avoid interactions between periodic images, in which half bottom atoms are fixed to simulate the bulk structure. Cu-doped $BiVO_4$ slabs were simulated by replacing two Bi atoms with Cu atoms. A Monkhorst-Pack k-mesh of $3 \times 3 \times 1$ k-points were used in the structural relaxation for all models.

Adsorption energies $E_{adsorption}$ are given with reference to the isolated surface $E_{surface}$ relaxed upon removing the molecule from the unit cell using identical computational parameters and the energy of the molecule $E_{molecule}$.

$$E_{adsorption} = E_{molecule\ on\ surface} - E_{surface} - E_{molecule} \quad (1)$$

Supplementary figures and tables

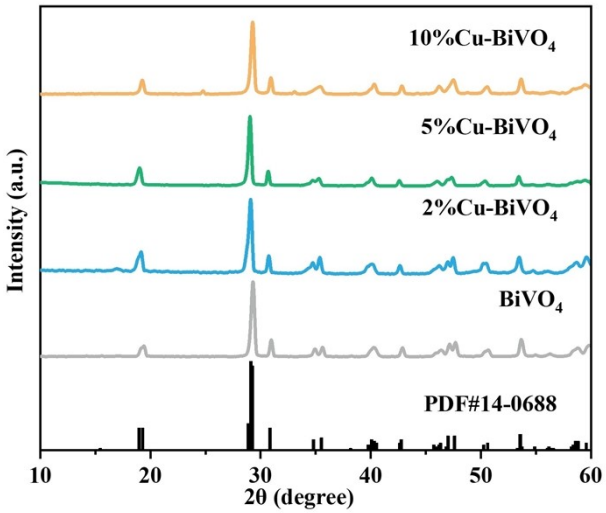

Figure S1. XRD patterns of the as-synthesized pristine $BiVO_4$ nanoplates and Cu-doped $BiVO_4$ nanoplates.

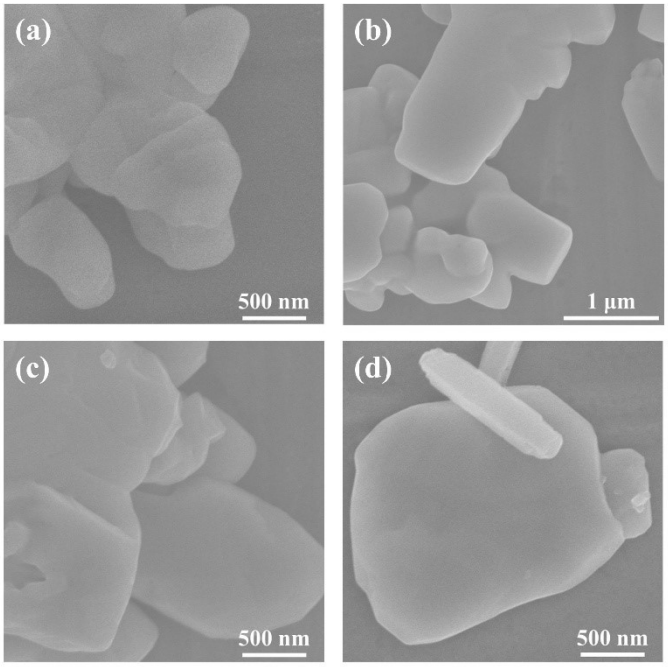

Figure S2. SEM images of the as-synthesized pristine $BiVO_4$ nanoplates and Cu-doped $BiVO_4$ nanoplates.

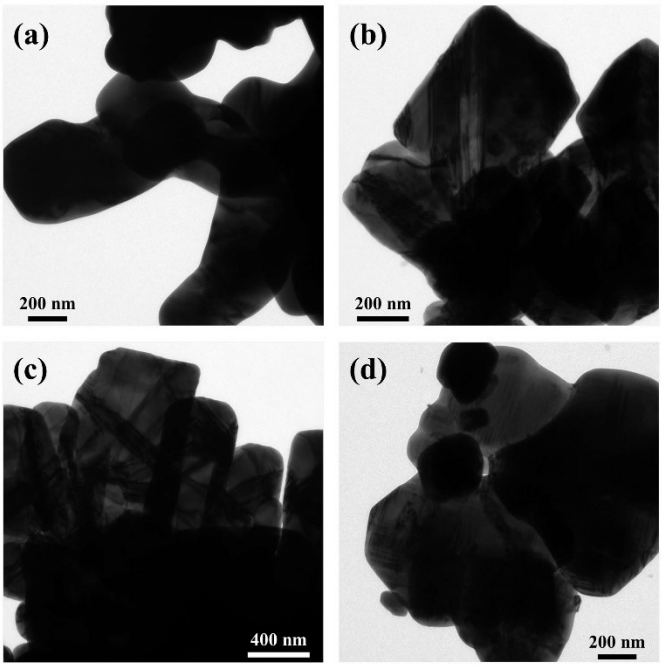

Figure S3. TEM images of the as-synthesized pristine $BiVO_4$ nanoplates and Cu-doped $BiVO_4$ nanoplates.

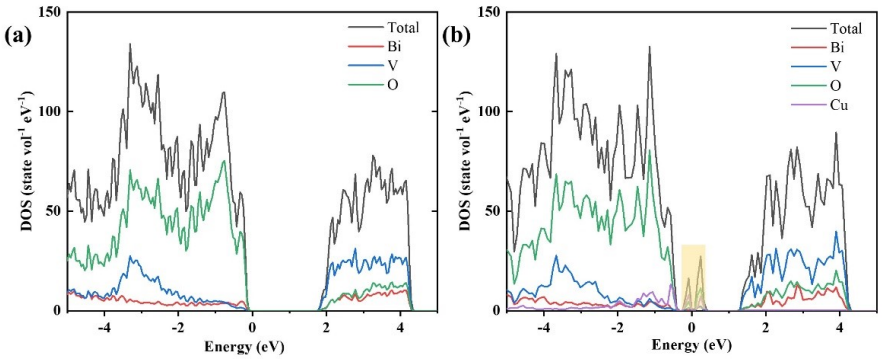

Figure S4. Calculated density of states for (a) the $BiVO_4$ nanoplates and (b) Cu-doped $BiVO_4$ nanoplates.

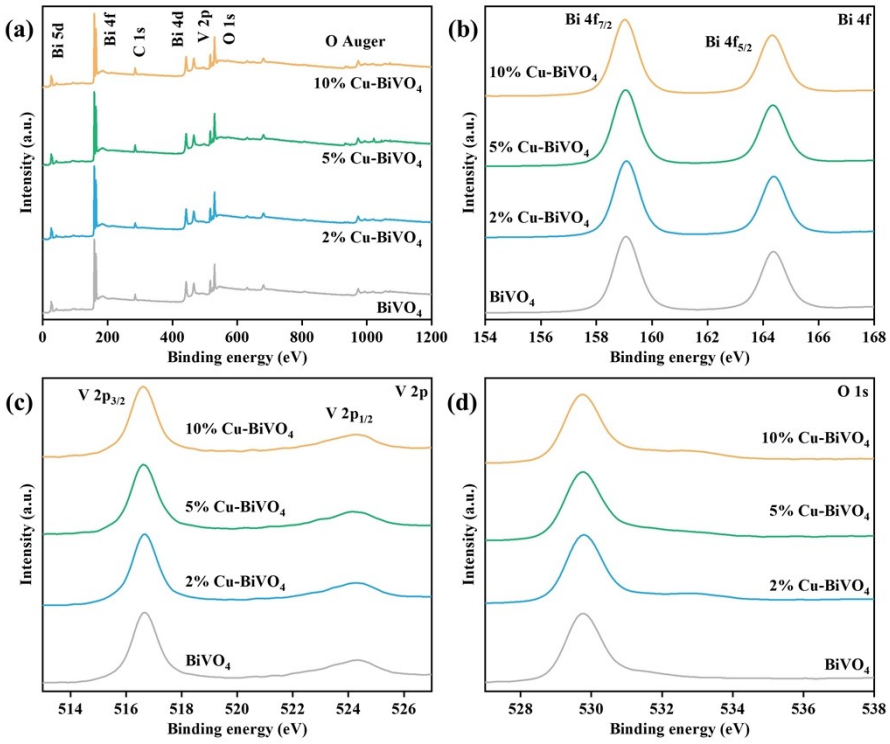

Figure S5. (a) The XPS survey spectra, (b) Bi 4f spectra, (c) V2p spectra and (d) O1s spectra of the as-synthesized pristine $BiVO_4$ nanoplates and Cu-doped $BiVO_4$ nanoplates.

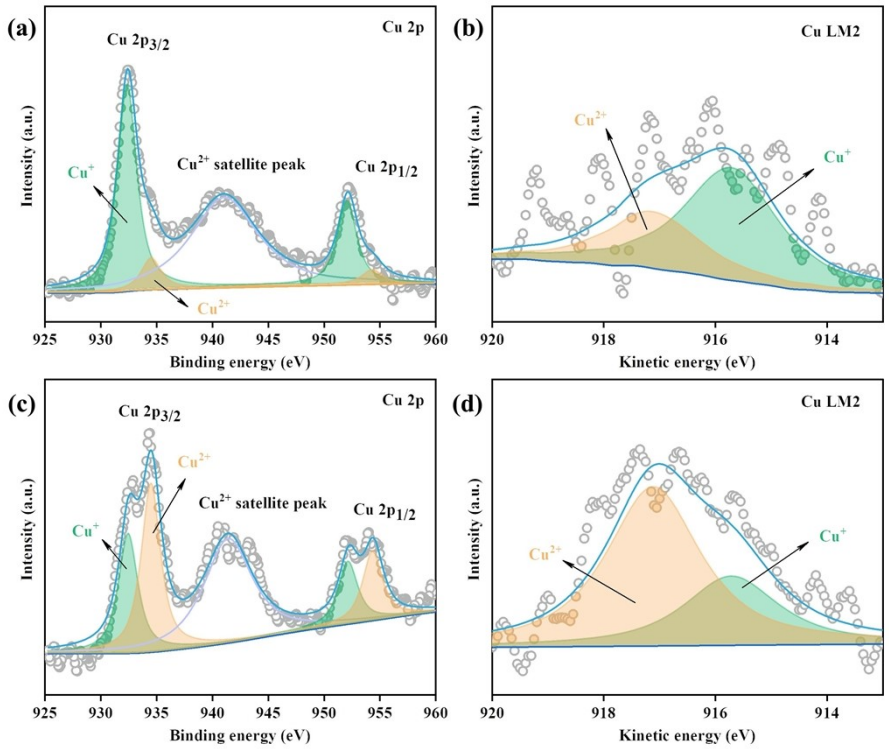

Figure S6. The Cu 2p and LM2 spectra of (a-b) the 2% Cu-doped $BiVO_4$ nanoplates and (c-d) 10% Cu-doped $BiVO_4$ nanoplates.

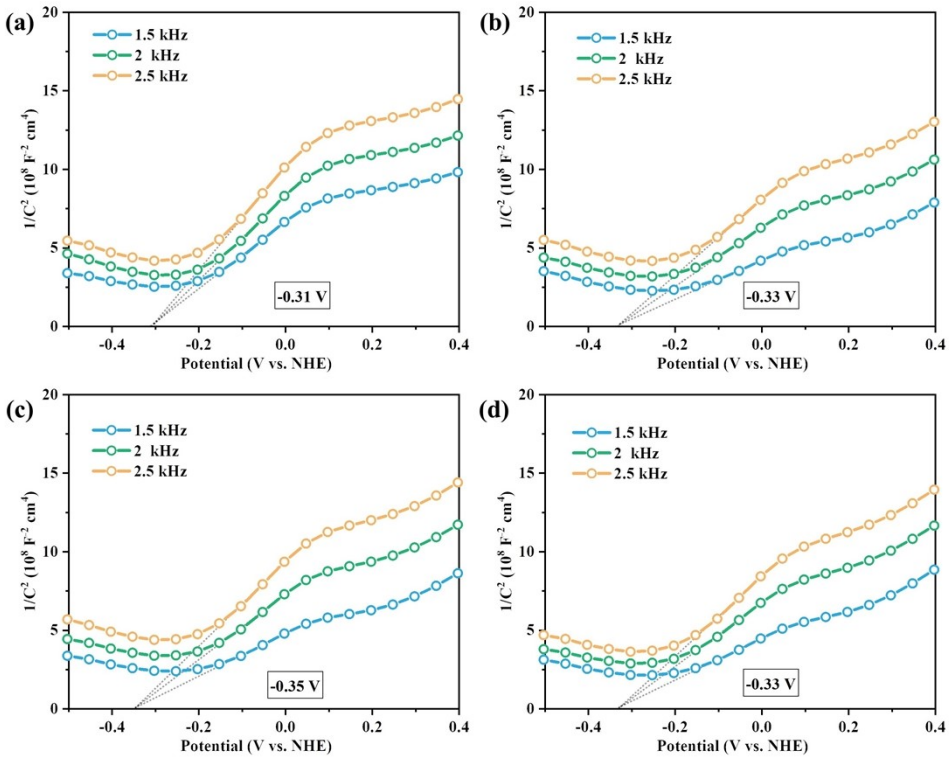

Figure S7. Mott−Schottky plots of (a) the pristine $BiVO_4$ nanoplates, (b) the 2% Cu-doped $BiVO_4$ nanoplates, (c) the 5% Cu-doped $BiVO_4$ nanoplates and (d) the 10% Cu-doped $BiVO_4$ nanoplates.

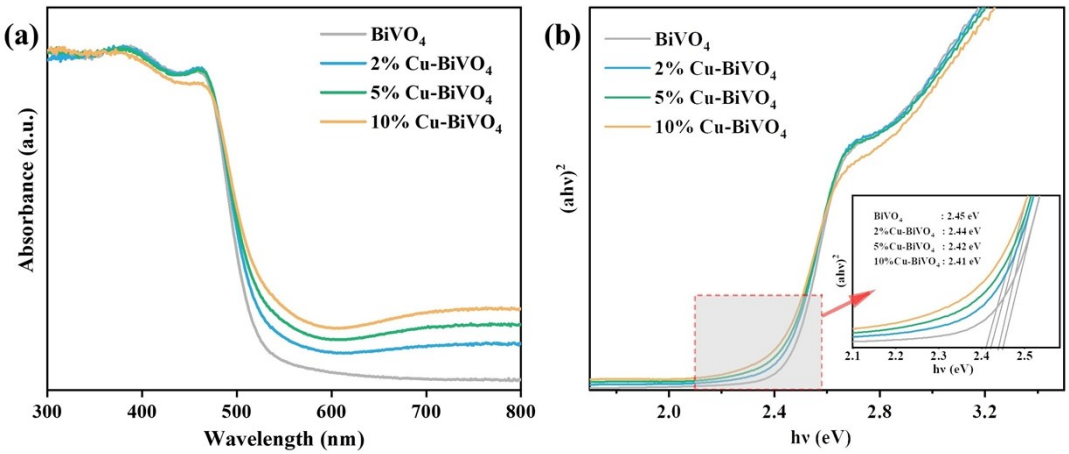

Figure S8. (a) UV–vis diffuse reflectance spectra of the as-synthesized pristine $BiVO_4$ nanoplates and Cu-doped $BiVO_4$ nanoplates. (b) The corresponding plotting $(\alpha h\nu)^2$ versus $h\nu$ to obtain bandgaps.

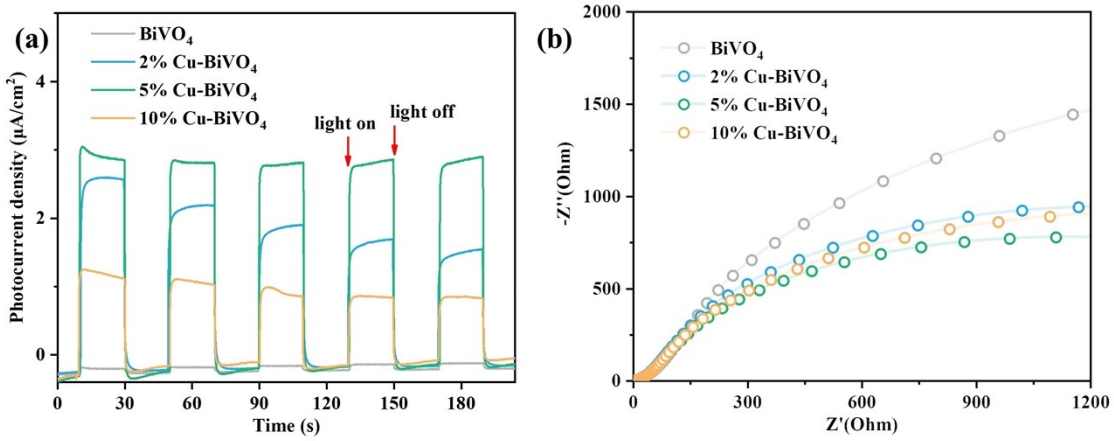

Figure S9. (a) The transient photocurrent response and (b) electrochemical impedance spectra (EIS) of the as-synthesized pristine $BiVO_4$ nanoplates and Cu-doped $BiVO_4$ nanoplates.

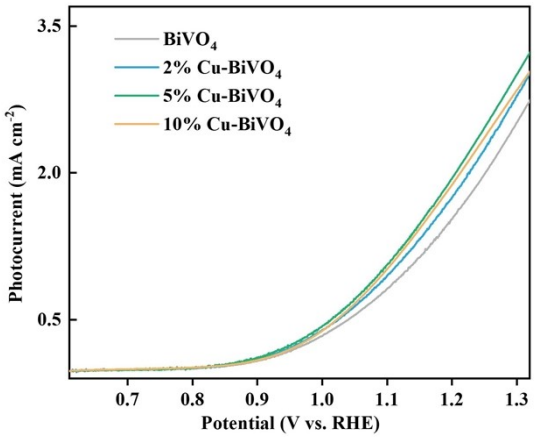

Figure S10. The photocurrent density measured in Na_2SO_3 electrolyte for the as-synthesized pristine $BiVO_4$ nanoplates and Cu-doped $BiVO_4$ nanoplates.

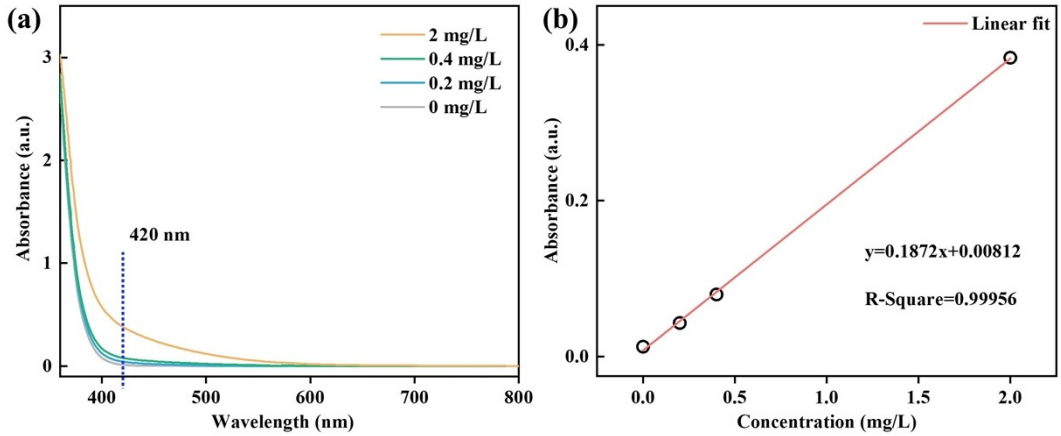

Figure S11. (a) UV-vis spectra of standard ammonia solutions via a Nessler's reagent method and (b) the corresponding standard curves for NH_4^+ quantitation.

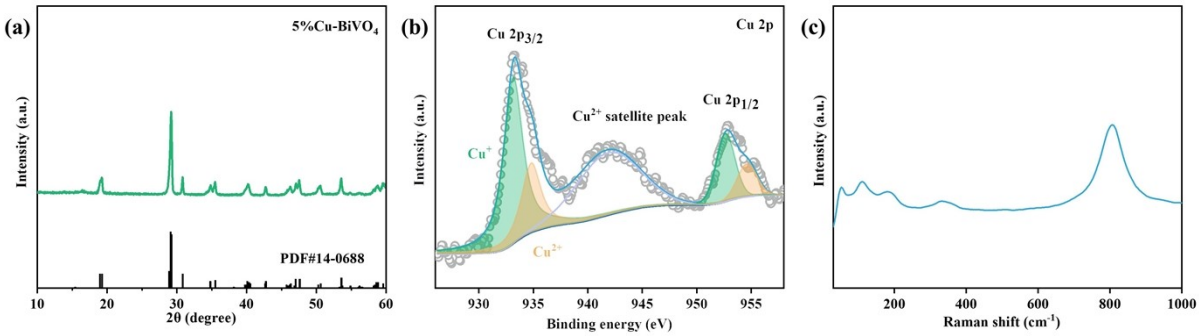

Figure S12. Characterizations for the 5% Cu-doped $BiVO_4$ nanoplates after the photocatalytic N_2 reduction. (a) XRD pattern, (b) the Cu 2p XPS spectrum and (c) the Raman spectrum.

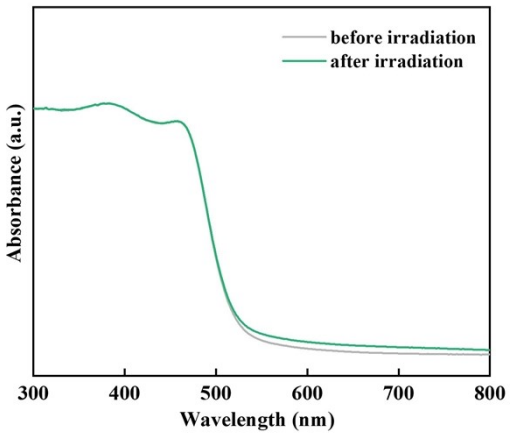

Figure S13. Quasi *in-situ* ultraviolet−visible diffuse reflectance spectroscopy (UV−vis DRS) for the pristine $BiVO_4$ nanoplates.

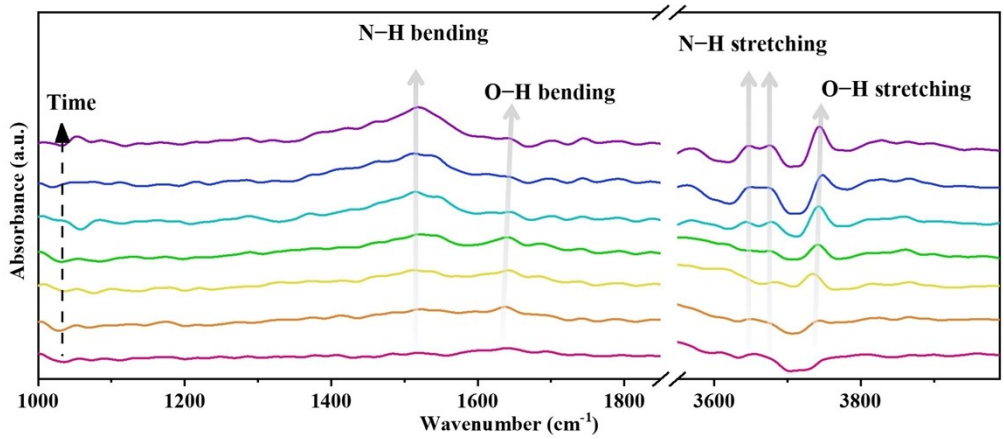

Figure S14. The *in-situ* FTIR spectra for the pristine $BiVO_4$ nanoplates under the same test conditions as the 5% Cu-doped $BiVO_4$ nanoplates.

Table S1. Comparison of photocatalytic ammonia generation rate with previously reported Bi-based photocatalysts.

Catalysts	Light source	Solution	Generation rate ($mM \cdot g^{-1} \cdot h^{-1}$)	Reference
Bi/Cu-Bi_2WO_6	Simulated solar	5 vol% MeOH aqueous	0.62	Ref. 6
Bi_2O_3/$CdMoO_4$	Simulated solar	5 vol% MeOH aqueous	0.32	Ref. 7
Bi/$PbBiO_2Br$	Simulated solar	5 vol% MeOH aqueous	0.24	Ref. 8
0.5 wt% Ru/$BiVO_4$	Full spectrum	Water	0.28	Ref. 9
MoS_2/In–Bi_2MoO_6	Full spectrum	Water	0.9	Ref. 10
0.50 wt% Pt/BiOBr	Full spectrum	Water	0.40	Ref. 11
$BiVO_4$/BiOCl	Visible light	Water	0.19	Ref. 12
5%Cu-$BiVO_4$	Full spectrum	1 vol% MeOH aqueous	2.94	**This work**
5%Cu-$BiVO_4$	Full spectrum	Water	0.82	**This work**

References

1. Liu, B., Wang, X., Zhang, Y., et al. Bismuth vacancies induced lattice strain in $BiVO_4$ photoanodes boosting charge separation for water oxidation. *Advanced Energy Materials*, **2025,** 15(17): 2403835.
2. Hodgetts, R. Y., Kiryutin, A. S., Nichols, P., et al. Refining universal procedures for ammonium quantification via rapid ^1H NMR analysis for dinitrogen reduction studies. *ACS energy letters*, **2020**, 5 (3): 736-741.
3. Kresse, G., and Furthmüller J. Efficiency of ab-initio total energy calculations for metals and semiconductors using a plane-wave basis set. *Computational materials science*, **1996**, 6 (1): 15-50.
4. Perdew, J. P., Burke, K., and Ernzerhof, M. Generalized gradient approximation made simple. *Physical review letters*, **1996**, 77 (18): 3865-3868.
5. Grimme, S., Antony, J., Ehrlich, S., and Krieg, H. A consistent and accurate ab initio parametrization of density functional dispersion correction (DFT-D) for the 94 elements H-Pu. *The Journal of chemical physics*, **2010**, 132 (15): 154104.
6. Li, X., Zhao, C., Wang, J., et al. Cu-doped Bi/Bi_2WO_6 catalysts for efficient N_2 fixation by photocatalysis. *Frontiers of Chemical Science and Engineering*, **2023**,17(10): 1412-1422.
7. Yuan, S., Wang, J., Zhao, C., et al. S-scheme $Bi_2O_3/CdMoO_4$ hybrid with highly efficient charge separation for photocatalytic N_2 fixation and tetracycline degradation: Fabrication, catalytic optimization, physicochemical studies. *Separation and Purification Technology*, **2023**, 325: 123665.
8. Dong, R., Yuan, S., Xu, J., et al. One-step preparation of Bi nanoparticles modified $PbBiO_2Br$ nanosheets with enhanced photocatalytic performance in N_2 fixation. *Solar Energy*, **2025**, 298: 113662.
9. Ren, G., Zhao, Z., Li, Z., et al. Rapid Joule-Heating fabrication of oxygen vacancies and anchor of Ru clusters onto $BiVO_4$ for greatly enhanced photocatalytic N_2 fixation. *Journal of Catalysis*, **2023**, 428:115147.
10. Ma, T., Li, R., Huang, Y., et al. Interfacial chemical-bonded $MoS_2/In–Bi_2MoO_6$ heterostructure for enhanced photocatalytic nitrogen-to-ammonia conversion. *ACS Catalysis*, **2024**, 14(8): 6292-6304.

11. Ren, G., Shi, M., Li, Z., et al. Electronic metal-support interaction via defective-induced platinum modified BiOBr for photocatalytic N_2 fixation. *Applied Catalysis B: Environmental*, **2023**, 327: 122462.
12. Han, Z., Sun, J., Ren, H. Spatially limited growth of ultrathin $BiVO_4$/BiOCl heterostructures in molten salt as effective nitrogen photofixation photocatalyst. *Journal of Alloys and Compounds*, **2025**,1049: 185450.